42th AIAA Plasmadynamics and Lasers Conference AIAA-2011-3281
27 – 30 Jun 2011, Honolulu, HI

Passive Mitigation of Aero-Induced Mechanical Jitter of Flat-Windowed Turrets

Zach B. Ponder[1], Stanislav Gordeyev[2], Eric J. Jumper[3]
University of Notre Dame, Notre Dame, IN, 46556

Steven Griffin[4]
Boeing-SVS Inc., Albuquerque, NM, 87109

and

Christopher McGaha[5]
Wright-Patterson AFB, AFRL/RBAI, Dayton, OH, 45431

Extensive experimental studies of mechanical vibrations or jitter imposed by a complex flow on a turret with a flat-window aperture were performed. The main goal of this investigation was to test passive flow control, such as pins upstream of the flat window and to document their impact on an overall turret jitter for different azimuthal angles of 73, 90, and 125 degrees. Local measurements of unsteady pressure on the surface of the turret for all tested configurations were conducted. Also, independent measurements of the turret jitter were conducted using a turret-mounted 3-axis accelerometer, three load cells placed on the base of the turret and a Malley probe, which measured laser beam deflections off a mirror attached to the flat window. It was shown that small and medium pins arranged in a single row were the most effective configurations in reducing the overall jitter of the turret. The physical mechanism of the flow control effect on the turret jitter is proposed and discussed. Finally, a finite-element model was built to predict turret jitter. Using experimentally-obtained unsteady pressure, the model confirmed the mitigation effect of the pin configurations.

I. Introduction

THE use of laser platforms on aircraft is typically implemented through the use of a hemisphere-on-cylinder turret, which provides a large range of elevation and azimuthal angles. However, from the aerodynamic point of view, the turret represents a bluff body and creates a very complex flow structure around the turret [1]. Inevitably, the flow separates from the turret, creating large unsteady vortices. These vortices result in fluctuations in the lift and the drag created by the turret, which can also result in vibrations, causing an overall optical beam to vibrate at primarily low frequencies. The problem is further amplified when a flat-window aperture is used on the turret, which creates a surface slope discontinuity and the formation of a unsteady separation bubble over a portion of the flat window [2-5]. Therefore, the otherwise collimated beam must pass through a variable-index-of-refraction field caused by the unsteady pressure wells created by this region of separated flow, eventually leading the optical beam becoming aberrated. Not only will these aberrations degrade the beam's ability to be focused in the far field, but the presence of the separated bubble over the flat window also creates unsteady force fluctuations which will in turn

[1] Graduate Student, Department of Aerospace and Mechanical Engineering, Hessert Laboratory for Aerospace Research, Notre Dame, IN 46556, AIAA Student Member.
[2] Research Associate Professor, Department of Aerospace and Mechanical Engineering, Hessert Laboratory for Aerospace Research, Notre Dame, IN 46556, AIAA Senior Member.
[3] Professor, Department of Aerospace and Mechanical Engineering, Cushing Hall of Engineering, Notre Dame, IN 46556, AIAA Fellow.
[4] Boeing Technical Fellow, Boeing-SVS Inc., Albuquerque, NM, 87109.
[5] Program Manager, Capt., USAF, AFRL/RBAI, Dayton, OH, 454311.

create additional vibration sources for the turret, usually at higher frequencies than the shedding frequency behind the turret. When these excitations couple into the beam-train steering mechanisms inside the turret, it can represent large displacements in the centroid of the beam over long distances, thereby severely limiting turret-based laser systems to be used for communications, interrogation, targeting, or direct-energy applications. As mentioned previously, high-order effects of the beam passing through variable-index-of-refractions created by density fluctuations caused by the aircraft-related flow itself, like the flow around an airborne turret is referred to as the aero optics problem. The second case, in which the beam is deflected due aero-optical distortions or vibrations of the turret and its components result in a deflection of the beam, is referred to as beam jitter.

This paper explores the jitter caused by vibrations of the flat-window turret due to unsteady forcing from the flow. Also the paper is focused on vibration mitigation strategies using passive-flow-control techniques such as an installation of passive vorticity-generating devices including small pins on the surface of the turret upstream of the flat window. These vorticity-generating devices were used to energize the boundary layer on the surface of the turret and to delay or modify/eliminate the separation bubble over the flat window. To investigate this, several sensors were used to measure the vibrations of the base and hemispherical portion of the turret. Direct measurements of the unsteady pressure fluctuations on the turret were performed and the net unsteady vibrations of the base of the turret were measured with load cells. Beam jitter was measured directly using a Malley probe, which is sensitive to both aero-optical jitter due to flow-related density fluctuations and mechanical vibrations of the turret.

II. Experimental Set-Up

The tests were conducted in the Subsonic Atmospheric Research Laboratory (SARL) in-draft facilities at Wright-Patterson Air Force Base, OH. A hemisphere-on-turret cylinder turret with a flat window was installed in the test section, which measures 7 feet wide by 10 feet tall, see Figure 1, top left plot. The turret diameter was 24 inches and the base height was 8 inches, so that the total turret height was 20 inches. The flat-window aperture was 12 inches in diameter. An aluminum splitter plate was attached to the floor of the tunnel to eliminate effects from the boundary layer formed on the floor of the wind tunnel. The mounting adapter plate was directly attached to the existing model pedestal located on the floor of the SARL wind tunnel. This adapter plate was fixed in its orientation with respect to the wind tunnel (wind direction), while the model was attached to the adapter plate with a series of screws so the turret model could be rotated about the center axis by loosening screws and rotating the turret model relative to the adapter plate; this setup allowed the ability for continuously changing the azimuthal angle of the model.

The turret was instrumented with six piezo-microphones located at the flat-window aperture to measure unsteady pressures over the aperture, see Figure 1, top right plot. One 3-axis accelerometer was mounted inside of the turret near the top to measure mechanical vibrations of the turret. The turret was attached to the stationary adapter plate via three load cells to also measure mechanical vibration of the turret, although at a different location. In addition to these sensors on the turret to directly measure mechanical vibrations, the mechanical vibration of the turret and the aero-optical environment around the turret at different azimuthal angles and the impact of the tested configurations were investigated non-intrusively using a Malley probe [4] for which a 1”-diameter flush-mounted flat mirror was placed close to the middle of the flat window, see Figure 1, top right plot. The schematic of the experimental optical setup is presented in Figure 2.

The baseline and several passive flow control configurations were tested at 5 azimuthal angles of 73, 85, 90, 110, and 125 degrees at one fixed elevation angle of 28 degrees at M = 0.3. Varying-length pin arrangements were mounted to the turret, as shown in Figure 1, bottom plot, along two rows of threaded holes ¾” apart on both sides of the flat window to provide different pin spacing and row arrangements: the inner row had holes with a spacing of ¾” and the outer row had holes with a spacing of 3/8”. For each configuration, either “small”, 1/2” tall, or “medium” ,3/4” tall, 3/16”-diameter pins were attached to the turret in a given pattern. Table 1 provides a description of each configuration. Unused holes were sealed with tape to prevent air leakage from inside the turret that would create synthetic jets.

For each run, all microphones, the 3-axis accelerometer, three force sensors and the Malley probe were simultaneously recorded with a sampling rate of 50 kHz twice for 15 seconds each.

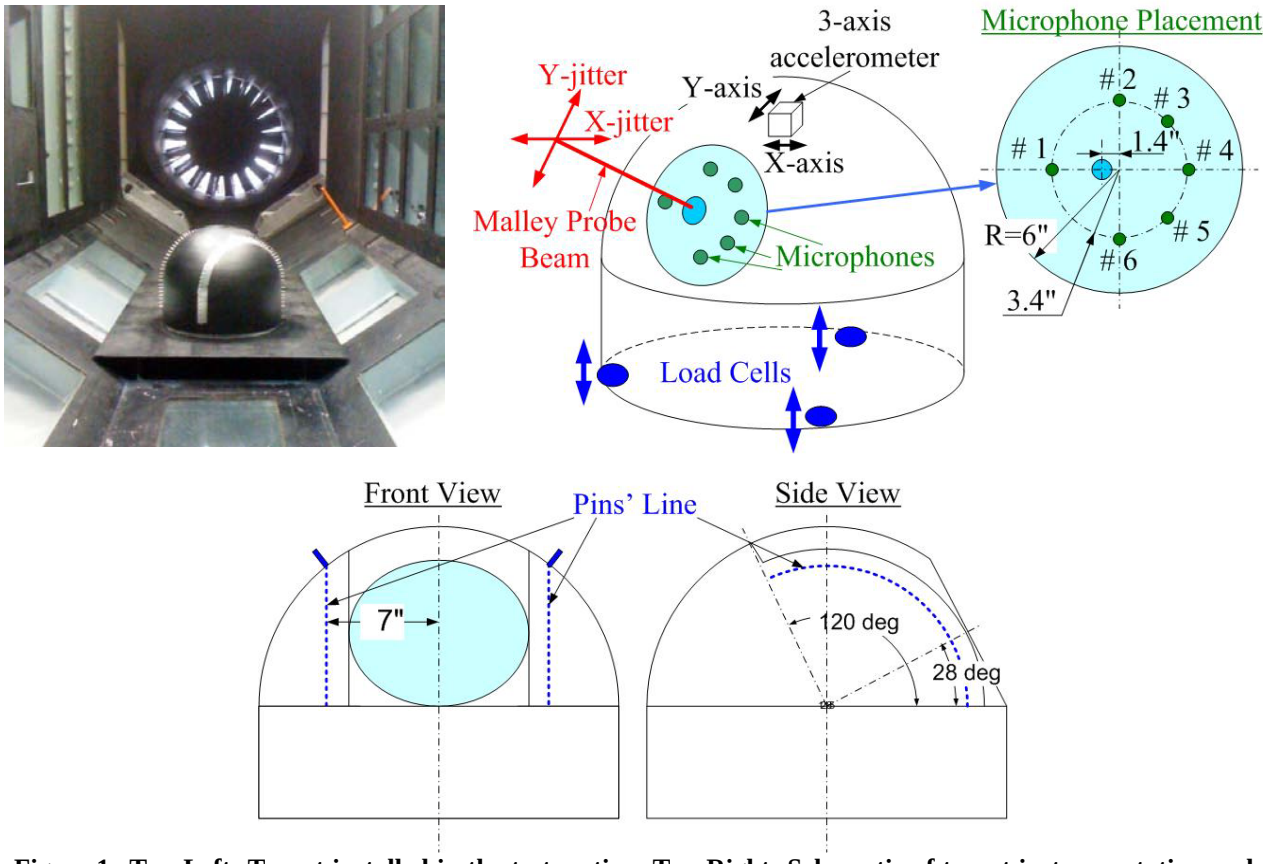

Figure 1. Top Left: Turret installed in the test section. Top Right: Schematic of turret instrumentation and microphone locations on the flat window. Bottom: Location of passive control devices (pins) on the turret.

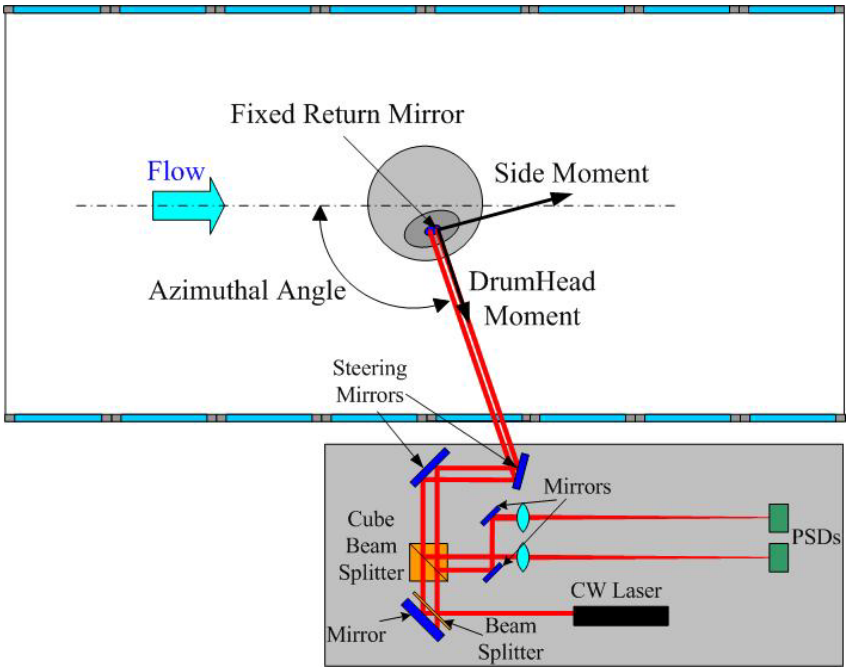

Figure 2. Malley probe optical setup and definition of moments acting on the turret.

Table 1. Tested Configurations

Configuration #	Configuration Description	Short abbreviations used in paper
1	Baseline (no passive flow control)	Baseline
2	¾" pins, ¾" spacing, inner row only	¾ Pins
3	½" pins, ¾" spacing, inner row only	½ Pins
4	½" pins, ¾" spacing, inner and outer rows, staggered	½ Pins, Staggered
5	½" pins, ¾" spacing, inner and outer rows, aligned	½ Pins, Aligned
6	¾" pins, 1.5" spacing, inner row only	Sparse
7	¾" pins, ¾" spacing, inner and outer rows, aligned ***90, 110, 125 degrees only***	¾ Pins, Aligned

III. Proposed Physical Mechanism for Jitter

The effect of the flat-window of the turret on aero-optical effects was intensively studied in several previous studies. In [4] aero-optical effects at back-looking angles (azimuthal angles above 90 degrees) were measured with the Malley Probe. Simultaneous velocity-optical measurements over the flat window showed the presence of the separated shear layer over the flat-window aperture. The effect of the slope discontinuity around the flat window was extensively experimentally studied both aero-optically and hydrodynamically for back-looking angles using a simplified version of a 2-dimensional cylindrical turret [5]. It was discovered that for elevation angles around 100 degrees a small unsteady separation bubble was present at the front portion of the flat window, which created additional optical distortions at these angles. Extensive aero-optical measurements around the flat-window turret at different azimuthal and elevation angles were performed in series of flight tests [6] and the presence of the small separation bubble at the front portion of the flat window at forward-looking angles between 70 and 90 degrees was also observed in aero-optical data; this unsteady bubble created small-scale turbulent structures and related increased levels of aero-optical distortions traveling over the flat window at these viewing angles.

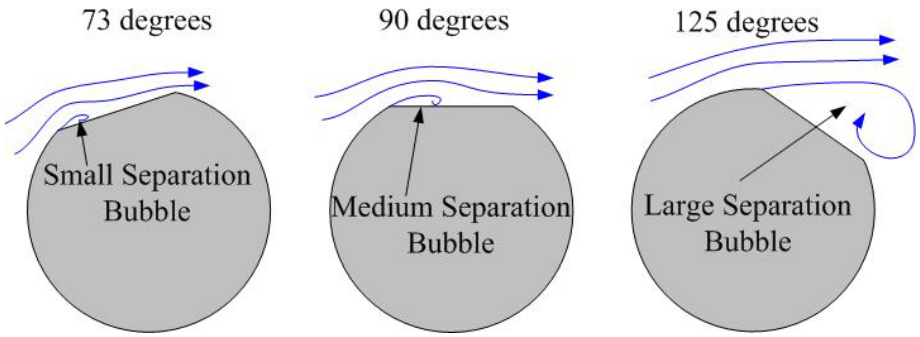

Figure 3. The flow topology around the flat-window turret at different viewing angles along the horizontal plane through the middle of the flat window.

Based on all these experimental evidences and observations, the flow topology over the flat-window turret for different viewing angles is schematically sketched in Figure 3. The scope discontinuity between the flat window and the turret body forces the flow to separate at viewing angle larger than 70 degrees; but for forward-looking angles the favorable pressure gradient over the flat window re-attaches the flow shortly after its separation, forming the small unsteady separation bubble. The bubble grows bigger as the favorable pressure gradient weakens when the viewing angle approaches 90 degrees. For back-looking viewing angles above 90 degrees the pressure gradient becomes adverse and the separation bubble grows larger and at some point becomes an open separation region.

At the range of viewing angles between 70 and 90 degrees the unsteady separation bubble is relatively small and sensitive to the incoming boundary layer. Preliminary aero-optical results [2,3] showed that the separation bubble can be significantly reduced or even eliminated and related aero-optical distortions reduced when the incoming boundary layer is energized by placing different passive devices, like rows of small pins upstream of the flat window.

All of cited references considered primarily unsteady aero-optical effects traveling over the flat-window turret. This paper investigates how rows of pins located upstream of the aperture effect the aero-optical and the mechanical jitter of the flat-window turret at different forward- and back-looking viewing angles.

IV. Results

A. Pressure results

Baseline unsteady-pressure spectra for the microphone # 1 located upstream of the middle of the flat-window for azimuthal angles of 73, 85, 90, 110, and 125 degrees are shown in Figure 4. The peak at approximately 150 Hz and its harmonic at 300 Hz are tunnel-related and correspond to the motor blade passing frequency. Unsteady pressure spectra went up with the azimuthal angle increasing between 73 and 90 degrees with a significant unsteady pressure spectrum amplitude at frequencies around 1 kHz, and then started decreasing at these high frequencies for higher azimuthal angles of 110 and 125 degrees. These results indicate that the level of unsteady pressure acting on the flat window of the turret was the highest between approximately around 90 degrees. These observations are consistent with the flow topology outlined in Figure 3, as the unsteady separation bubble grows larger but still had a finite size at the azimuthal angle of 90 degrees.

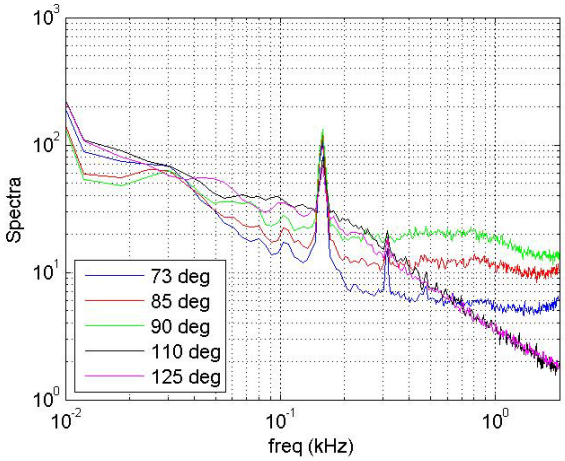

Figure 4. Unsteady pressure spectra for Mic # 1 for baseline case at different azimuthal angles.

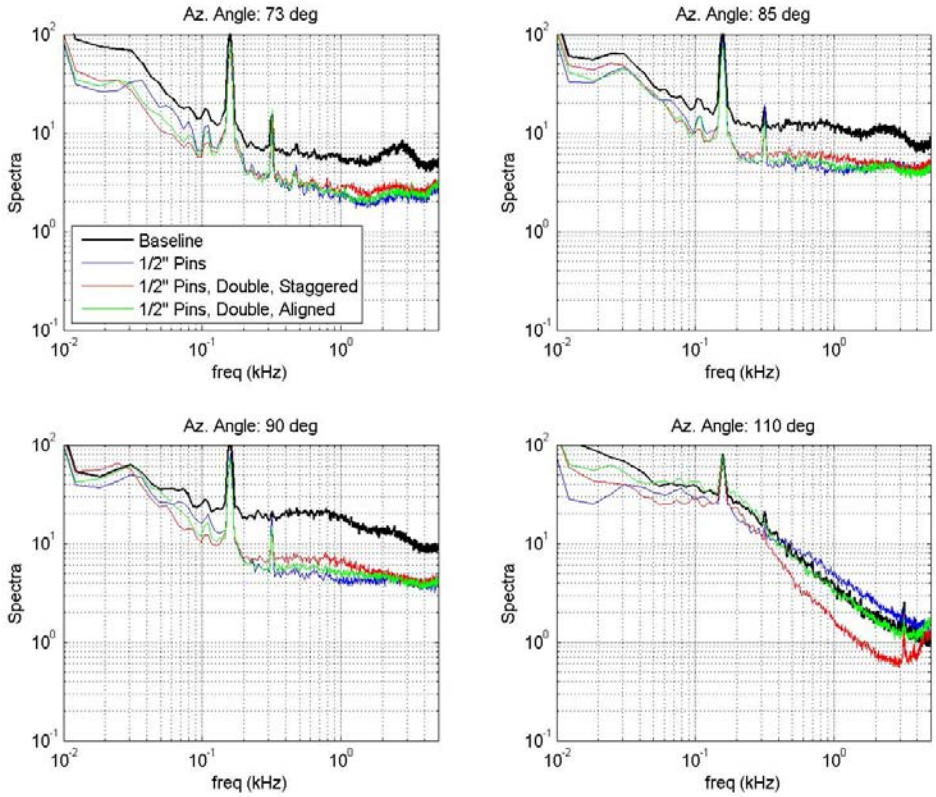

Figure 5. Unsteady pressure spectra for Mic # 4 for baseline and several tested configurations for different azimuthal angles.

Unsteady pressure spectra for the microphone # 4 located downstream of the middle of the flat window for the baseline (no flow control) and selected pin configurations for different azimuthal angles are shown in Figure 5. As

mentioned before, two sharp peaks at 150 and 300 Hz for all cases are tunnel-motor related. For the 73-degree case, the significant spectra reduction over a wide range of frequencies was observed for all configurations. The single row of ½" pins provided the most unsteady pressure reduction up to approximately 1 kHz; above this frequency, double row of ½" pins was the most effective configuration. At the azimuthal angles of 85 and 90 degrees, all configurations reduce the unsteady pressure levels over a wide frequency range; the double row of ½" staggered pins and the double row of ¾" aligned pins (not shown) were slightly better when compared to other configurations. At the azimuthal angle of 110 degrees, all configurations energized the upcoming boundary layer and consequently reduce the separation region over the flat window, therefore reducing an overall level of unsteady pressure fluctuations. The spare single row of ¾" pins (not shown), the single row of ½" pins and the double row of ½" staggered pins were found to be the most effective in lowering the unsteady pressure spectra over a wide range of frequencies. All these results confirmed that the separation bubble is reduced fro forward-looking angles by variety of passive flow control.

B. Malley Probe Jitter

Figure 6, upper left plot, shows the results of the Malley-Probe X-jitter (the jitter component in the streamwise direction, see Figure 1, top left plot) for the azimuthal angle of 73 degrees for the baseline and several tested configurations. Almost all tested configurations modified the baseline spectrum, notably in the high-frequency region above 600 Hz for the X-jitter. For the X-jitter, "1/2 Pins, Aligned" provided no visible reduction in the beam jitter, while the "1/2 Pins" gave the most beam-jitter reduction for frequencies above 1kHz.

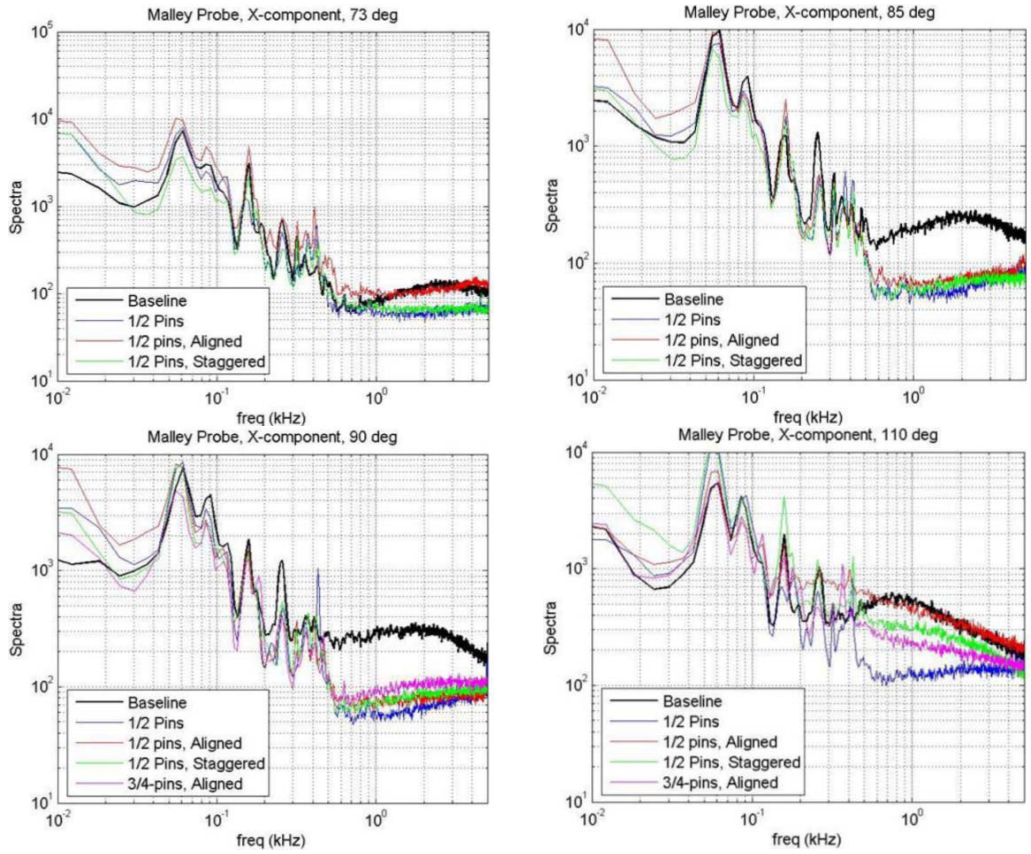

Figure 6. Malley probe beam x-component jitter spectra for baseline and selected pin configurations for different azimuthal angles. M = 0.3.

Jitter mitigation results were even more pronounced for the azimuthal angle of 85 and 90 degrees, presented in Figure 6, upper right and lower left plots, respectively. At these angles, all configurations significantly reduced the beam jitter for frequencies above 500 Hz; however, the single row of ½" pins were found to be the most effective configurations in improving the beam jitter at these angles.

As was discussed earlier, the flow was mostly attached over the flat window at the forward- and side-looking angles between 73 and 90 degrees, except for the small separation bubble just downstream of the surface discontinuity; small pins introduced strong streamwise vorticity into the attached boundary layer upstream of the flat window and the energized incoming boundary layer tended to re-attach the separated flow over the flat window sooner, compared to the baseline, when no pins were present. Analysis of the Malley probe results showed that small, ½" pins were the most effective in introducing a proper amount of turbulence into the boundary layer and therefore reduced the overall amount of aero-optical jitter and traveling aero-optical distortions. Other configurations involving either more pins, like double-row pins, or fewer pins, like the sparse pin configuration, were found to be less effective in reducing overall turret jitter.

In the interest of space, the remainder of analysis will compare the baseline and the 'best' configuration, which is a single line of 1/2" pins, labeled later as "1/2"-pins".

1. *Linear Stochastic Estimation*

The fact that the Malley probe is sensitive to both vibrational movement of the turret-mounted mirror and to changes in the aero-optical environment makes it difficult to separate the vibrational motion of the turret from the aero-optical effect of density variations. The model-mounted accelerometer and the load cells at the bottom of the turret, on the other hand, is sensitive to only the vibrational motion of the turret structure. By using the fact that accelerometers are sensitive only to the mechanical motion, a method called Linear Stochastic Estimation (LSE) was used to separate the jitter due to the mechanical motion of the turret from the aero-optically-induced jitter.

Originally applied to turbulent flows as a method of determined the existence of coherent structures, the LSE technique finds a conditionally-averaged value of some quantity when the prescribed event happens [7]. If the quantity is noted as $u_i(x; t)$, the event data vector (the given vector of variables with the associated event occurrence) is defined as E_j, and the conditional average is defined as $\langle u_i | E_j \rangle$, the LSE technique provides a linear estimation of the conditional average as

$$\hat{u}_i = \textit{linear estimate of } \langle u_i | E \rangle = L_{ij} E_j, \tag{1}$$

where the estimation coefficients, L_{ij}, are calculated from the system of equations,

$$\langle E_j E_k \rangle L_{ij} = \langle u_i E_k \rangle \tag{2}$$

Thus, using simultaneous measurements of the turret motion from both the accelerometer and load cells, which forms the event data vector, and the total beam jitter from the Malley Probe, the LSE technique provides an estimate of the mechanical part of the jitter. The difference between the total and the mechanical part of the jitter signal is an estimated aero-induced part of the jitter signal. Figure 7 shows an example of applying the LSE technique for the baseline case for the azimuthal angle of 90 degrees: the spectrum of the total jitter signal, the reconstructed mechanical part of the spectrum using the LSE technique, and finally the original jitter spectrum minus the reconstructed spectrum, which is called the aero-induced spectrum. As expected, the mechanical part of the jitter dominates the total jitter for low frequencies below 500 Hz, and the aero-induced jitter dominates at higher frequencies. The analysis of the phase difference between the aero-induced jitter for two Malley Probe beams (not shown) revealed that aero-optical component of the jitter represented the traveling aero-optical structure. After separating the mechanical and aero-induced parts of the total signal, each component can be analyzed separately.

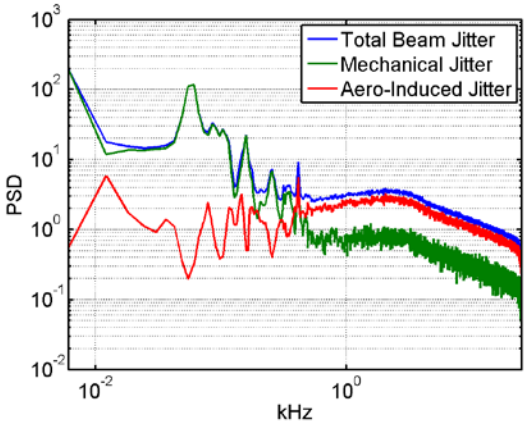

Figure 7. Malley probe Spectra illustrating the LSE procedure. Azimuthal angle is 90 degrees, X-jitter component only.

2. *Mechanical Part of Malley Probe Jitter*

Figure 8 shows the mechanical part of the Malley probe jitter signal for the baseline and the ½"-pins cases for different azimuthal angles. The greatest decrease in mechanical jitter is seen at the azimuthal angle of 73 degrees. This result is consistent with the global reduction of the unsteady pressure spectra over the flat window, shown in Figure 5. The effect of the passive flow control devices on the mechanical jitter is reduced as the azimuthal angle is increased and at the azimuthal angle of 125 degrees the pins do not improve the mechanical jitter of the turret; at this

look-back angle the flow separates at the front portion of the flat window and formed the open separation region, as schematically shown in Figure 3, and the flow remains separated even with the inclusion of the passive flow control.

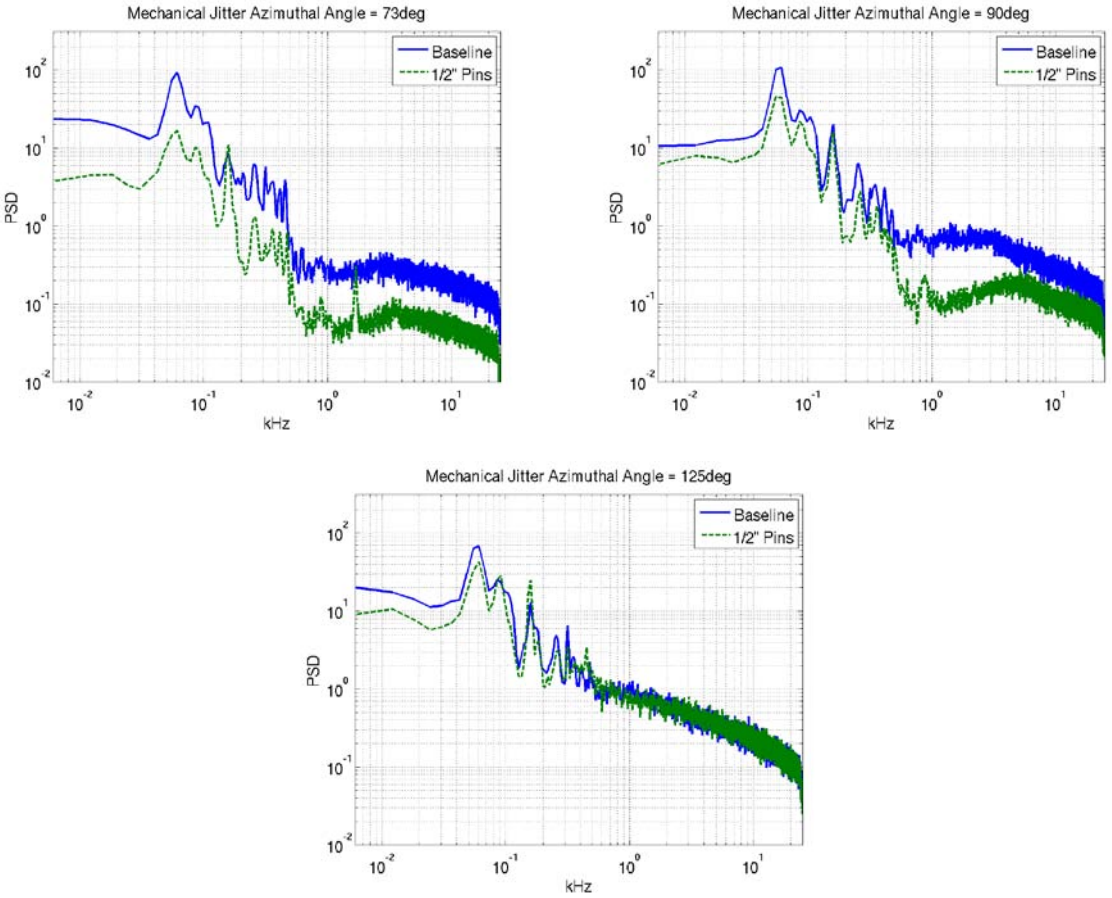

Figure 8. Comparison between mechanical part of the X-jitter component of Malley probe for baseline and controlled cases.

3. Angular Dependence of Aero-Optical Part

Examination of the aero-optical part of the Malley probe data as a function of the azimuthal angle with and without the passive flow control reveals some physical insight into the aero-optical structure at different azimuthal angles. Figure 9 shows the power spectra of the aero-optical part of the Malley probe for the baseline and ½"-pins configurations. For the azimuthal angle of 73 degrees, Figure 9, top left plot, there is a reduction in the power spectral density of the aero-optical part between the baseline and ½"-pin case. As expected, this is very similar with the analysis of the total Malley Probe jitter as seen in Figure 6, but with a reduced energy in the spectra in the lower-frequency range, showing the ability of the LSE technique to effectively separate the mechanical jitter from the aero-optical part. For the azimuthal angle of 90 degrees, Figure 9, top right plot, the flow control also significantly reduced the aero-optical portion of the Malley probe and shifted the location of the aero-optical peak from 2.5 kHz to 5 kHz. It implies that the streamwise size of the aero-optical structure was reduced by the flow control by the factor of two, so the flow control broke the underlying aero-optical structure into a smaller ones. For the azimuthal angle of 125 degrees, Figure 9, bottom plot, the strength of aero-optical structure was essentially unchanged by the flow control, while the dominant aero-optical peak was shifted from 1kHz to 0.5 kHz; thus, the flow control increased the size of the aero-optical structure at this azimuthal angle. Note that the aero-optical peak location of the baseline for about 3 kHz for 73 and 90 degrees, then was shifted toward a lower frequency of 1 kHz at 125 degrees. A possible explanation is that pins increased the thickness of the incoming boundary layer and therefore increased the size of the vortical structures in the shear layer. All of these observations are consistent with the proposed baseline flow topology, shown in Figure 3: at 73 and 90 degrees, the small separated bubble introduced small vortical structures into the flow, and the flow control disrupted the bubble and decreased the size of the aero-optical

structures. At the azimuthal angles of 125 degrees the large separated region was formed over the flat window, which created the shear layer with large characteristic aero-optical scales over the flat window.

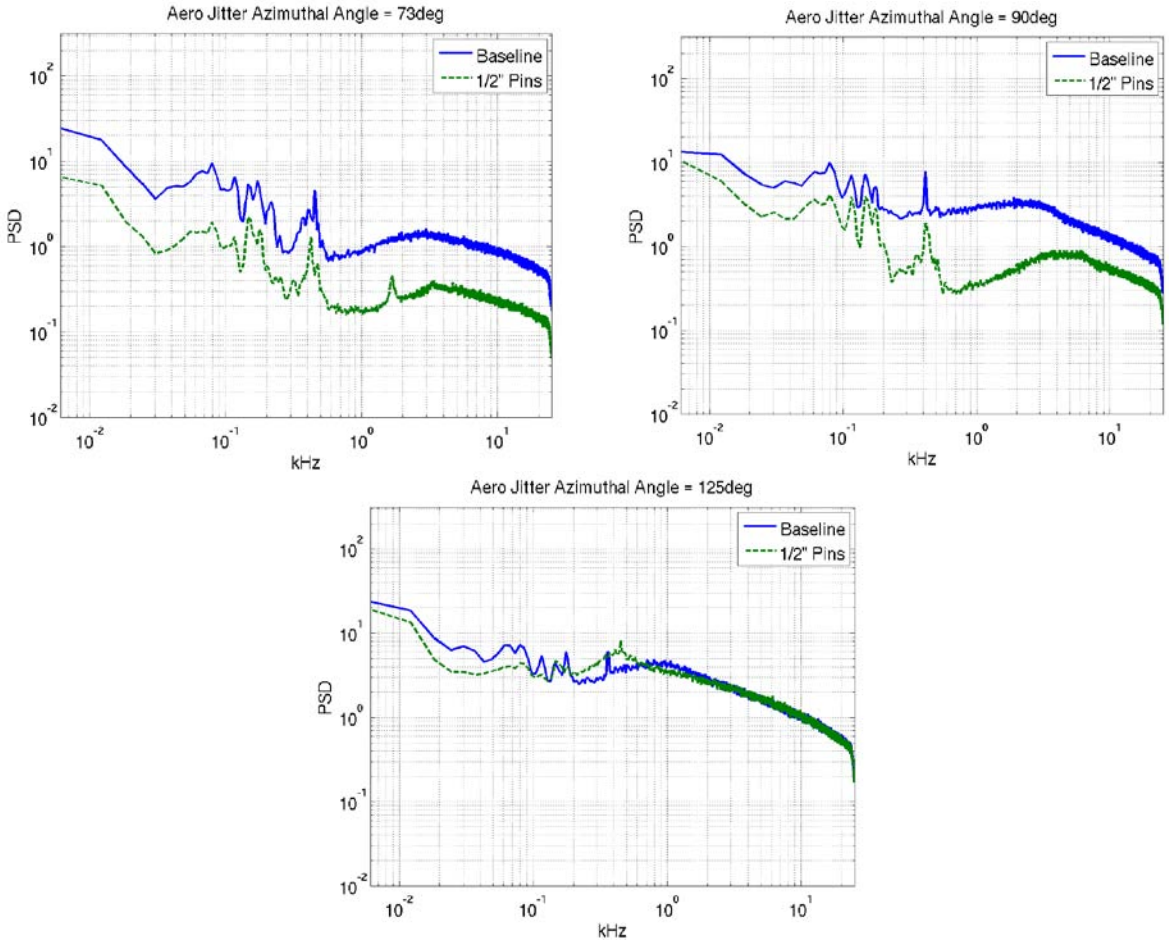

Figure 9. Comparison between aero-induced X-Jitter spectra for baseline and ½"-Pin-case for different azimuthal angles.

C. Cross-Correlations

Locally measured quantities such as the Malley probe jitter and unsteady pressure spectra do indicate an optimal pin sizing and arrangement. To gain a better understand of the global vibrational environment induced by the unsteady aerodynamic loading, we can turn our attention to cross-correlations between various sensors. Later in this paper we will consider an amplitude and a phase of a normalized spectral cross-correlation between different sensors.

Figure 10, left plot, shows calculated spectral cross-correlation for the baseline between the Y-component of the accelerometer this is in the direction normal to the flat window, (labeled as accel Y-axis in the figure), and microphone # 1 located upstream of the center on the flat window. Figure 5, right plot, presents the correlation results between the accelerometer Y-axis and the microphone # 1 for the ½"-pins case for the azimuthal angle of 90 degrees. For both cases the correlation was relatively high and in-phase at the lower frequencies between 10 and 60 Hz. The unsteady pressure and the turret motion were also correlated at tone frequencies of 150 and 300 Hz, as acoustical noise from the motor at these frequencies was creating the unsteady pressure field and the corresponding unsteady forcing acting on the turret. The pins increased the normalized correlation between the local pressure and the global turret motion in the range of frequencies between 10 and 300 Hz; this result can be interpreted as pins disrupting the formation of the small separation bubble over the flat window and forming a more global, though a weaker flow structure over the flat window. Higher frequencies in the pressure spectrum do not seem to cause any significant turret motion, probably due to an alternating-in-space pressure pattern on the flat window with less

resulting force acting on the turret. Figure 11 presents an example of correlation results between the Y-axis accelerometer located near the top of the turret and the 'drumhead' moment, calculated using load cells at the bottom of the turret. The 'drumhead' moment is the moment acting on the turret perpendicular to the flat window, as defined in Figure 2. Both signals were strongly correlated and were in-phase at the range of frequencies between 10 and 100 Hz, indicating that the turret moved as a rigid body at these low frequencies. The correlation is also relatively high at frequencies above 100 kHz, but a complicated amplitude and phase relations indicated the presence of many elastic modes excited in the turret shell.

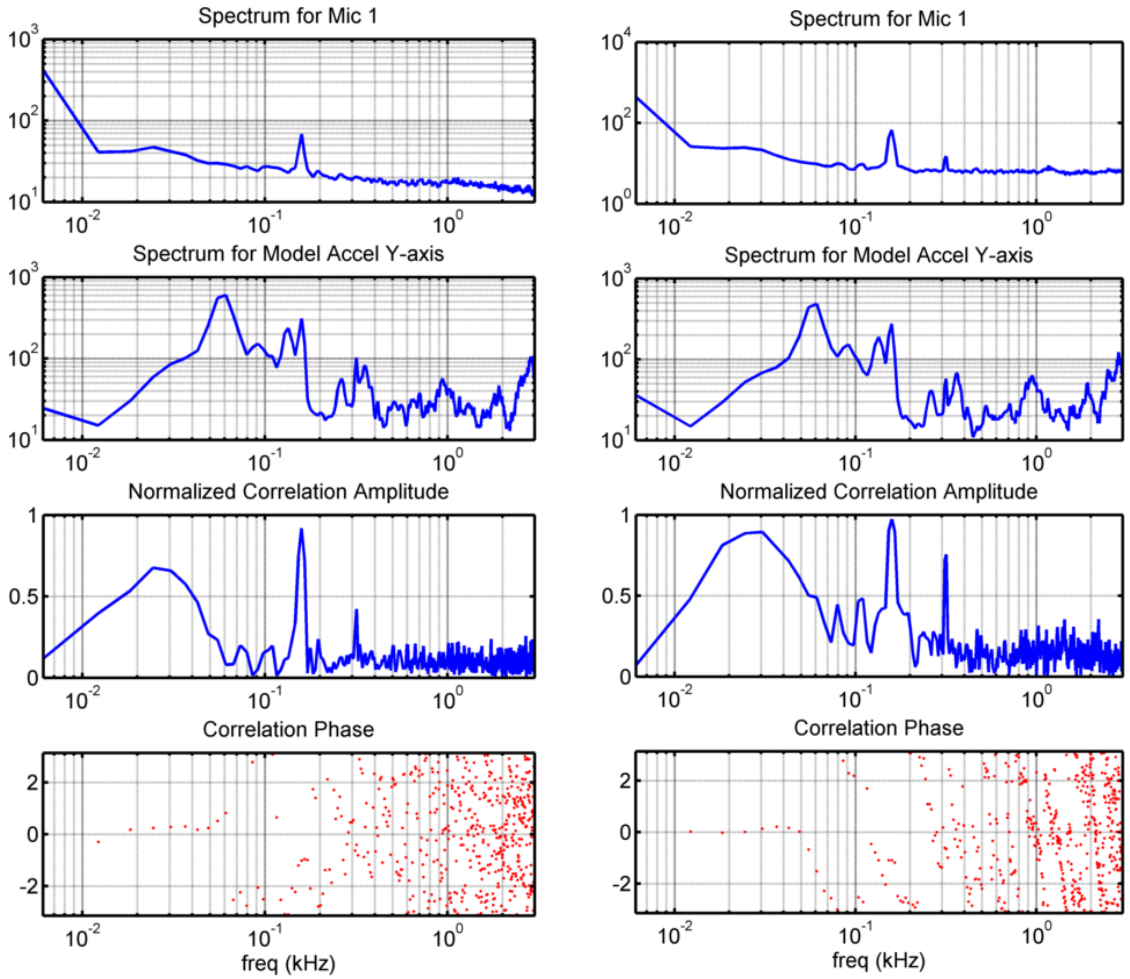

Figure 10. Spectral cross-correlation between the Mic # 1 and accelerometer Y-axis (aligned through flat window) for baseline case [left column] and ½"-pin case [right column]. Azimuthal angle is 90 degrees.

1. Cross-Correlation between aero-induced part of the Malley and pressure sensors

Analysis of the correlation between the aero-optical part of the Malley probe and microphones on the flat window provides a better understanding of the relationship between the aero-optical structure and the related pressure fluctuations on the surface of the flat window for the baseline and the flow control cases. Figure 12 shows the correlation for the aero-induced X-jitter and the upstream microphone # 1 for the baseline and the ½"-pins case. For the baseline, Figure 12, left plot the non-zero correlation was present in the range of frequencies between 0.5 and 5 kHz, with the linear phase variation. The linear dependence of the phase versus frequency indicates that the underlying structure was convecting between the two sensors. These sensors measure different quantities, surface pressure and density fluctuations, and the non-zero correlation indicated the presence of the coherent structure. A possible mechanism for forming the structure is that the unsteady separation bubble at the front portion of the flat window created significant turbulent vortical structures. These vortical structures convect over the flat-window aperture and effect both the wall-pressure, recorded by the microphone and density field, measured by the Malley probe. The evidence of these traveling structures at looking-forward angles between 70 and 80 degrees were

observed over the flat aperture in flight tests [6]. When the flow control was applied, it disrupted the formation of the separation bubble and these traveling structure were no longer present over the flat aperture. Figure 12, right plot, showed that indeed the correlation between the Malley probe and the microphone was essentially zero for the ½"-pins case.

The correlations between the aero-induced jitter and the downstream microphone #4 for the baseline and the flow control case for the azimuthal angle of 73 degrees are presented in Figure 13. For the baseline, the correlation also showed the presence of the traveling structure over the downstream portion of the flat window. Note that the phase slope was negative, as the microphone was downstream of the Malley probe. The level of the correlation is smaller compared to the correlation level between the microphone # 1 and the Malley Probe. One reason is that the distance between the microphone # 1 and the Malley Probe was approximately 2 inches, while the distance between the microphone # 4 and the Malley Probe was almost 5 inches, thus making correlations weaker. The correlation between the downstream microphone and the Malley probe for the ½:-pins case is presented in Figure 13, left plot. The correlation was even smaller, compared to the baseline case, although the linear phase suggested some signs of the weak travelling structure.

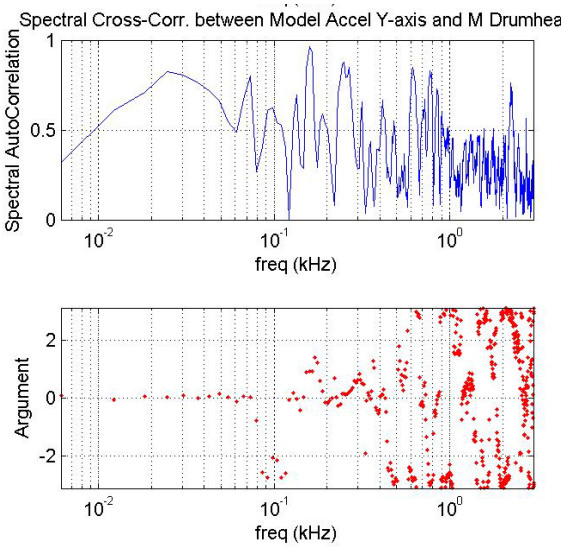

Figure 11. Cross Correlation between the Model accel Y-axis and the 'Drumhead' moment for baseline case, azimuthal angle of 90 deg.

Based on the relative distances between the microphones # 1, #4 and the Malley probe and using the time delays calculated for the phase slopes for the baseline case from Figures 12 and 13, left plots, the convective speed of the aero-optical structure was estimated at approximately 105 m/sec, or roughly the freestream speed. This value of the speed is consistent with direct measurements of the speed of aero-optical structures reported in [6].

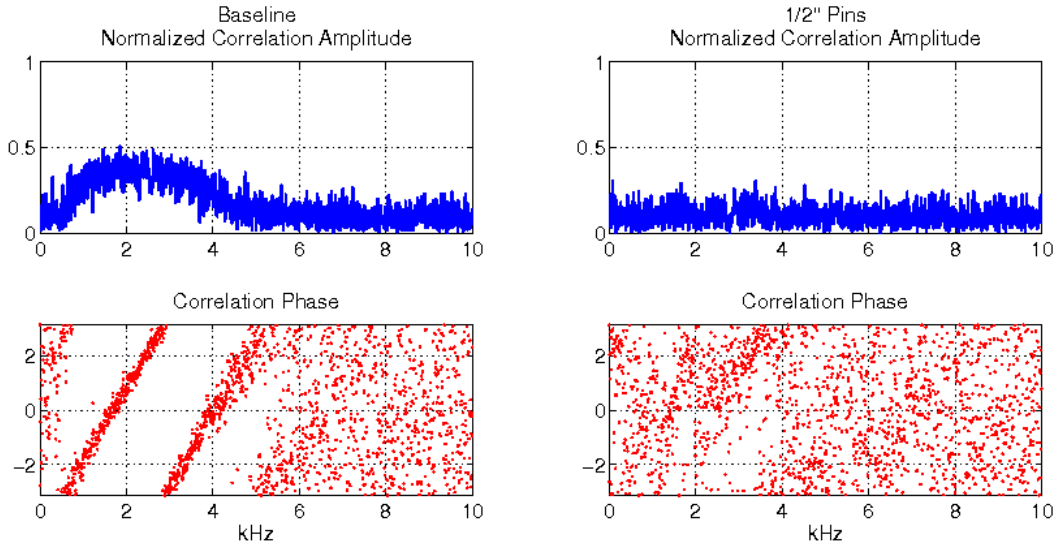

Figure 12. Cross Correlation between the Microphone # 1 (upstream of middle of the aperture) and Aero-induced X-jitter for baseline case (left column) and ½ Pins-case (right column). Azimuthal angle is 73 degrees.

Results of the correlation between microphones # 1 and # 4 and the Malley probe jitter at the azimuthal angle of 90 degrees for the baseline and the controlled case are presented in Figures 14 and 15. For the baseline case, the results are very similar in nature to the baseline results for the azimuthal angle of 73 degrees, presented in Figures 12 and 13, although the correlation levels between the forward-located microphone # 1 and the Malley Probe were

stronger at this azimuthal angle at the range of the frequencies between 1 and 5 kHz; the flow control significantly reduced the correlation, implying the disruption of the separation bubble. The phase slope, though, was about the same for both the baseline and the flow control case, meaning that the flow control changed the intensity of the aero-optical structure, but not its speed. The calculation of the convective speed at this azimuthal angle gave the value of approximately 130 m/sec, or 1.24 of the freestream speed. Note the local speed on top of the turret is higher than the freestream speed due to the flow blockage by the turret. For the conformal-window turret, for instance, the local speed on top of the turret is 1.5 times faster than the freestream speed. Using this number as an estimate of the local speed over the flat window gives the ratio between the convective speed of the aero-optical structure and the local speed as 0.82. This number is very close to the normalized convective speed observed in the subsonic attached boundary layer [8]. Again, this is consistent with the boundary-layer-like velocity profile observed on the flat window of the cylindrical turret at 90 degrees [5].

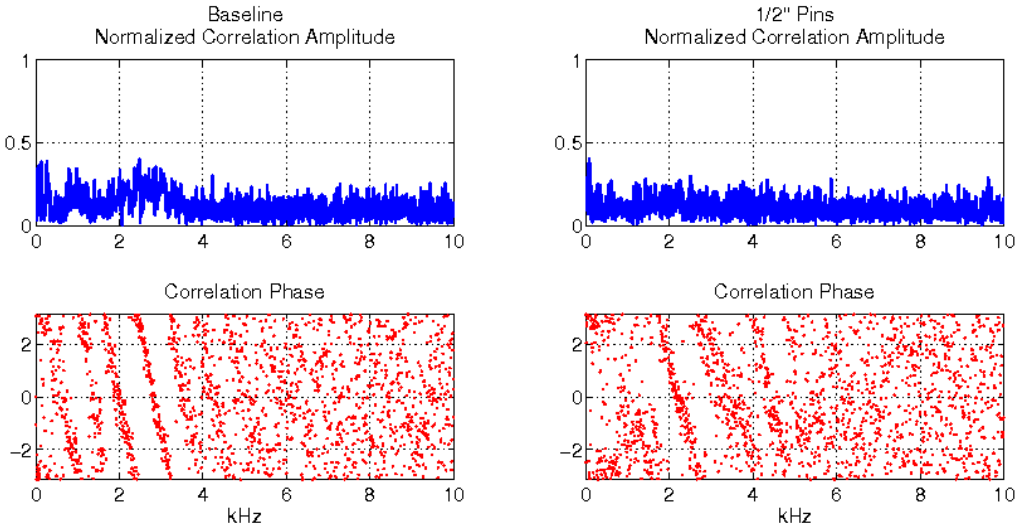

Figure 13. Cross Correlation between the Microphone # 4 (upstream of middle of the aperture) and Aero-induced X-jitter for baseline case (left column) and ½ Pins-case (right column). Azimuthal angle is 73 degrees.

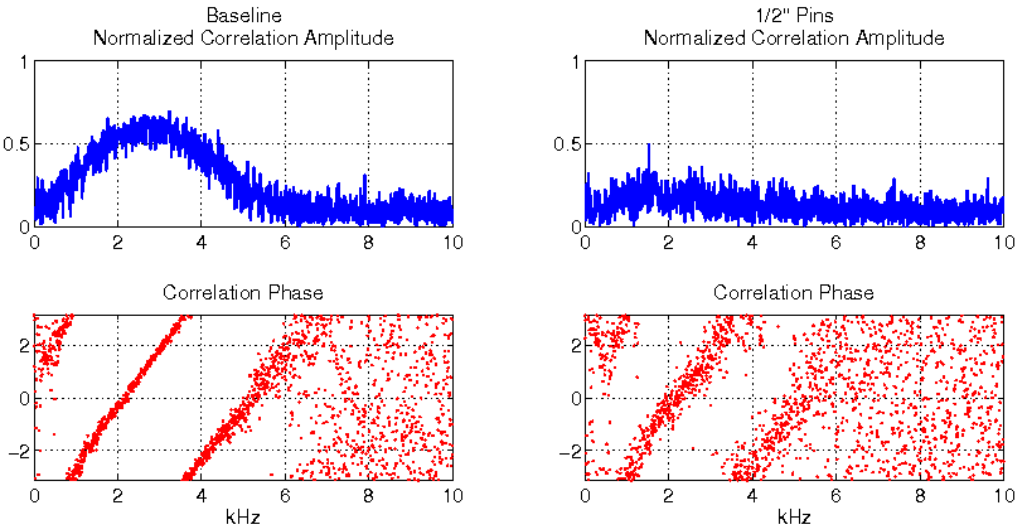

Figure 14. Cross Correlation between the Microphone # 1 (upstream of middle of the aperture) and Aero-induced X-jitter for baseline case (left column) and ½ Pins-case (right column). Azimuthal angle is 90 degrees.

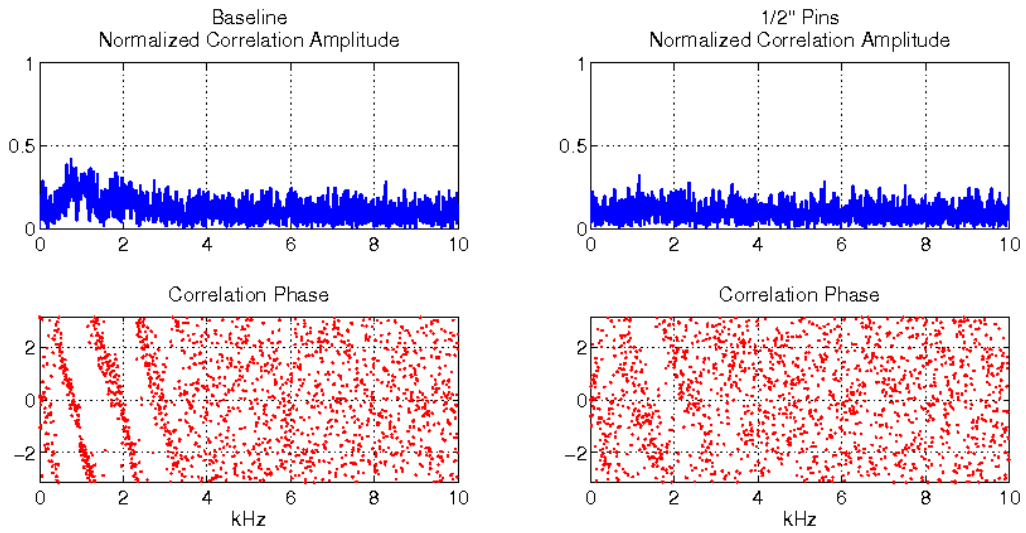

Figure 15. Cross Correlation between the Microphone # 4 (upstream of middle of the aperture) and Aero-induced X-jitter for baseline case (left column) and ½ Pins-case (right column). Azimuthal angle is 90 degrees.

Results of the correlation between the microphones # 1 and # 4 and the Malley probe for the baseline and the flow control cases for the azimuthal angle of 125 degrees are shown in Figures 16 and 17. Note, that the frequency axis is presented in logarithmic-scale for this angle. For the microphone # 1 and the Malley probe the non-zero correlation range was located at lower frequencies between 0.4 and 2 kHz. The flow control shifted this range to smaller frequencies between 0.2 and 0.8 kHz. It is consistent with the observation in Figure 9, bottom plot, that the flow control moved the location of the aero-optical peak from 1 kHz for the baseline to approximately 0.5 kHz for the flow control case, indicating the increase in size of the aero-optical structure via possibly increasing the thickness of the incoming boundary layer. The flow control also increased the level of the correlation, indicating a stronger aero-optical structure. The correlation between the downstream microphone # 4 and the Malley probe is weak for both the baseline and the flow control cases, as the shear layer moved away from the flat window, so the wall-pressure became less correlated with the aero-optical structure in the shear layer.

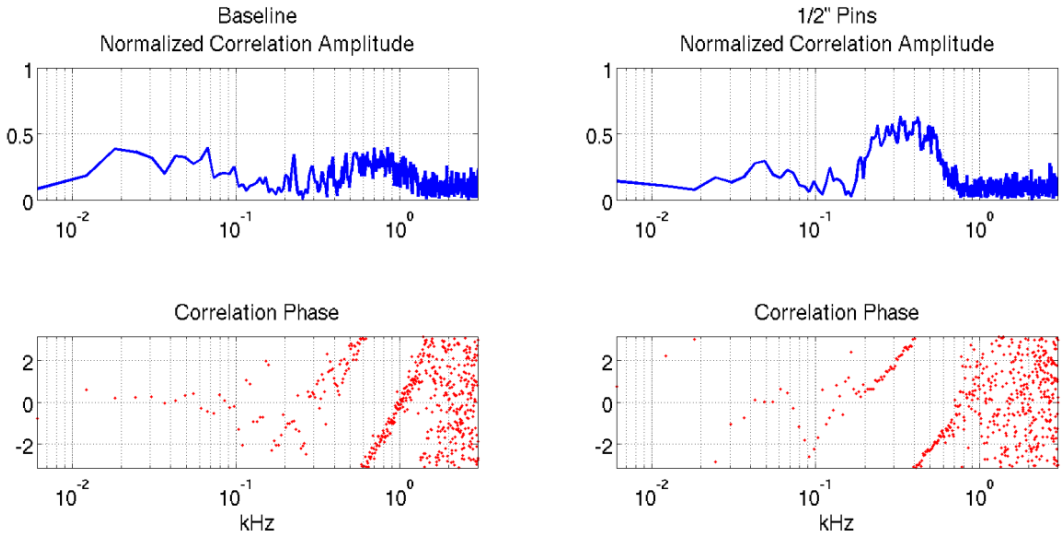

Figure 16. Cross Correlation between the Microphone # 1 (upstream of middle of the aperture) and Aero-induced X-jitter for baseline case (left column) and ½ Pins-case (right column). Azimuthal angle is 125 degrees.

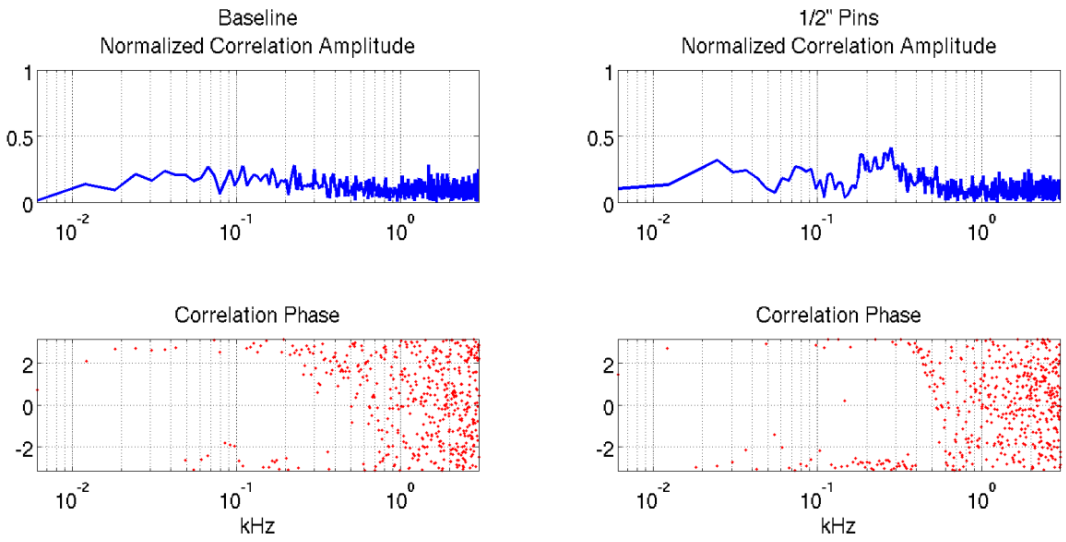

Figure 17. Cross Correlation between the Microphone # 4 (upstream of middle of the aperture) and Aero-induced X-jitter for baseline case (left column) and ½ Pins-case (right column). Azimuthal angle is 125 degrees.

D. Structural Response Model

An integrated structural/optical/controls model was to used to predict closed-loop optical jitter for different passive flow control configurations. The model incorporated an optical ray trace and structural finite element model for a turret-based laser system with geometrical characteristics matching the turret tested. The model also included inertial stabilization of the turret and fast steering mirror stabilization of the optical path. Previous use of the integrated model with pressure inputs generated by an unsteady computational fluid dynamics (CFD) model and base disturbance inputs from flight measurements had produced closed loop optical jitter predictions that agreed with measured flight data with less than 15% RMS error.

The inclusion of the active control system in the integrated model for passive flow control was intended to weight performance due to approaches that were most effective at improving performance on the laser system. Microphone data were used as pressure inputs to the model in place of the CFD generated inputs. Depending on assumptions made about how to map the measured pressure data to the nearest nodes on the finite element model, a range of predicted reductions in closed loop optical jitter was calculated. There was also an assumption made that only the loading on the nodes near the microphones changed with the flow control, and the pressure over the rest of the turret was unaltered. The calculations were performed for only one azimuthal angle of 85 degrees. Results in the normalized form (the baseline response was set to one) are presented in Table 2. The ½" pins, a single row were predicted to reduce closed loop jitter by as much as 71%. Maximum predicted reduction in jitter for double rows of pins was found to be around 64%.

Table 2. Predicted normalized turret mechanical response for selected configurations

Baseline	½” Pins	½” Pins, Double, Staggered	½” Pins, Double, Aligned
1.0	0.29-.62	0.36-.65	0.37-.65

V. Conclusion

The effect of passive flow control devices in form of small cylindrical pins placed upstream of the flat window has been investigated on a hemisphere-on-cylinder with the flat-window aperture for different azimuthal angles. An optimization of pin length, spacing, and arrangement was performed in order to minimize an overall mechanical jitter of the turret. Dynamic surface pressure measurements were made using microphones at several locations on the turret. Beam jitter measurements, containing both aero-mechanical jitter and aero-optical disturbances near the center of the flat window were recorded using the Malley probe. Analysis of spectra of different local quantities, such as pressure and Malley Probe, and global quantities, like the mechanical jitter of the turret, as well as various spectral cross-correlations was preformed. The results support the following conclusions: for large forward-looking

angles between 70 and 90 degrees the small separation bubble was formed downstream of the slope discontinuity between the upstream portion of the flat window and the turret body. This unsteady separation bubble introduced turbulent structures, convecting downstream, which in turn, increased the unsteady pressure fluctuations and the resulting mechanical jitter of the turret. The pins introduced the additional vorticity and momentum into the incoming boundary layer, reduced the size of the separation bubble and, consequently reduced the size and strength of the turbulent structures and, therefore, reducing the overall pressure levels over the flat window and the overall mechanical jitter of the turret. For the look-back angle of 125 degrees, the flow separated at the front edge of the flat window and formed the shear layer over the flat window. The flow control thickened the incoming boundary layer and increased the size of the vortical structures inside the shear layer, but did not change the turret mechanical jitter. Finally, a finite-element model used the experimentally-measured pressures to predict the overall jitter of the turret. The model confirmed that the flow control was efficient in reducing the total level of the mechanical jitter of the turret.

Acknowledgments

These efforts were sponsored by the Air Force Research Laboratory under Contract Number PO#AFRL0000000263 and Boeing Purchase Contract #120337 with support from the Subsonic Aerodynamic Research Laboratory (SARL) at Wright-Patterson AFB, OH. The U.S. Government is authorized to reproduce and distribute reprints for governmental purposes notwithstanding any copyright notation thereon.

The authors would like to thank the SARL personnel, especially Oliver Leembruggen for providing technical assistance during tests. Also, we would like to thank Jacob Cress and Christopher Porter for their help collecting experimental data.

References

[1] Gordeyev, S., Jumper, E.: Fluid Dynamics and Aero-Optics of Turrets. *Progress in Aerospace Sciences* **46**, 388-400 (2010)

[2] Gordeyev, S., Jumper, E., Ng, T., Cain, A.: The Optical Environment of a Cylindrical Turret with a Flat Window and the Impact of Passive Control Devices. AIAA Paper 2005-4657 (2005)

[3] Cress, J., Gordeyev, S., Jumper, E., Ng, T., Cain, A.: Similarities and Differences in Aero-Optical Structure over Cylindrical and Hemispherical Turrets with a Flat Window. AIAA Paper 2007-0326 (2007)

[4] Gordeyev, S., Hayden, T., Jumper, E.: Aero-Optical and Flow Measurements Over a Flat-Windowed Turret. *AIAA Journal* **45**, 347-357 (2007)

[5] S. Gordeyev, J.A. Cress, E. Jumper and A.B. Cain.: Aero -Optical Environment Around a Cylindrical Turret with a Flat Window. *AIAA Journal*, **49**(2), pp. 308-315 (2011)

[6] Porter, C., Gordeyev, S., Zenk, M., Jumper, E.: Flight Measurements of Aero-Optical Distortions from a Flat-Windowed Turret on the Airborne Aero-Optics Laboratory (AAOL), 42nd AIAA Plasmadynamics and Lasers Conference, Honolulu, HI, 27-30 June 2011, AIAA Paper 2011-3280. (2011)

[7] Adrian, R.: On the role of conditional averages in turbulent theory. *Turbulence in Liquids: Proceeedings of the 4th Biennial Symposium on Turbulence in Liquids*, 322-332 (1977)

[8] S. Gordeyev, E. Jumper and T. Hayden.: Aero-Optics of Supersonic Boundary Layers**.** AIAA Paper 2011-1325 (2011)